https://doi.org/10.1016/j.jallcom.2017.11.355

Low-temperature-sintered Pr-doped 0.93($Bi_{0.5}Na_{0.5}$)TiO_3-0.07$BaTiO_3$ multifunctional ceramics with Li_2CO_3 sintering aid

Tat-Hang Chung and K.W. Kwok*

Department of Applied Physics

The Hong Kong Polytechnic University, Kowloon, Hong Kong, China

Keywords: Pr-doped BNTBT; sintering aid; photoluminescence; ferroelectrics; piezoelectric properties

* Corresponding author. Tel.: +852 27665667; fax: +852 23337629.

E-mail address: apkwkwok@polyu.edu.hk (K.W. Kwok)

Abstract

Multifunctional ceramics with good dielectric, ferroelectric, piezoelectric and photoluminescence properties have been fabricated at a low sintering temperature of 960°C. Via the addition of Li_2CO_3, oxygen vacancies are produced in the Pr-doped $0.93(Bi_{0.5}Na_{0.5})TiO_3$-$0.07BaTiO_3$ ceramics, which can enhance the ionic lattice-diffusion coefficient, promote the densification and thus lower the sintering temperature effectively from 1200 to 960°C. The Li-addition also induces lattice distortion and expansion, which strengthen the internal field among the polar nano-regions of the ceramic. As a result, the depolarization temperature is increased and the room-temperature piezoelectric properties are enhanced. Moreover, the structural symmetry is reduced, and thus leading to an increase in the uneven components of the crystal fields around Pr^{3+} and then an enhancement in photoluminescence emissions. Together with the good dielectric properties assured by the dense structure, the ceramics are ready for use in multifunctional optoelectronic applications.

1. Introduction

Multifunctional materials possessing two or more desirable properties have attracted considerable attention and become the interdisciplinary field of research [1,2]. Ferroelectric materials possesses strong piezoelectric properties have been extensively studied for developing new multifunctional materials such as multiferroics with strong ferroelectric and magnetic properties. Recently, there are growing interests of developing materials possessing strong piezoelectric and photoluminescence (PL) properties for multifunctional optoelectronic applications [3-5]. Rare-earth ions are commonly doped in a ferroelectric host for realizing the PL emissions. However, there are usually adverse effects on the ferroelectric and piezoelectric properties.

Ferroelectric materials are characterized by their switchable spontaneous polarization and their capabilities of, after orienting the spontaneous polarizations to a direction (i.e., poling), producing electric charges in response to an external stress (i.e., piezoelectric effect) or dimensional deformation under an external electric field (i.e., converse piezoelectric effect). Because of the good piezoelectric properties, lead-containing ferroelectric ceramics, such as lead zirconate titanate, have widely been used in various sensor and actuator applications. With the increasing concerns over lead-pollution, lead-free ferroelectric ceramics have recently been investigated extensively for replacing them. $(Bi_{0.5}Na_{0.5})TiO_3$ (BNT) is one of the most promising candidates that exhibits a high Curie temperature (T_C = 320°C), a high depolarization temperature (T_d = 180°C) and strong ferroelectricity (remanent polarization P_r = 38 $\mu C/cm^2$) [6, 7]. However, it has a high conductivity and coercive field (E_c = 7.3 kV/mm), which cause the poling extremely difficult and thus leads to a small piezoelectric coefficient d_{33} of 85 pC/N. A number of modified systems have then

been developed for improving the piezoelectric properties, such as BNT-$NaNbO_3$ [8], Bi_2O_3-doped BNT [9], $Bi_{0.5}(Na_{1-x-y}K_xLi_y)_{0.5}TiO_3$ [10] and (1-x)BNT-x$BaTiO_3$ (BNT-BT) [6,11]. Among them, BNT-BT exhibits the highest value of d_{33} (155 pC/N) near the morphotropic phase boundary, i.e., 6 - 7 molar % of BT. Although the T_d of the ceramic decreases to ~100°C following the tradeoff relationship between d_{33} and T_d normally existed in various BNT-based ceramics [12], it is still high enough for the ceramic to be used in various practical applications. Similar to other ferroelectric ceramics, the sintering temperature of BNT-BT is high (typically above 1200°C), which will induce volatilization losses of Bi and Na and thus degradation of piezoelectric properties [13,14]. It is then of great interest to lower the sintering temperature not only for eliminating the volatilization losses and improving the piezoelectric properties but also for reducing the production cost as well as protecting the environments. A number of liquid-phase sintering aids, such as V_2O_5 [15], Li_2CO_3-Bi_2O_3-$CdCO_3$ [16], $LiBiO_2$ [17] and Li_2CO_3 [18,19] have been shown effective in lowering the sintering temperature of various piezoelectric ceramics to below 1000°C. Such a low sintering temperature also allows the ceramics to be co-sintered with Ag/Pd 30/70 instead of platinum inner electrodes in fabricating multi-layered structures that have been widely used for various actuator and transformer applications. In general, the liquid formed in the early stage of sintering can wet the sold grains, increase the mass transport rate and then promote the grain coarsening and densification of the ceramics [20]. However, the liquid will form a secondary phase and generally degrade the electrical properties of the ceramics [21].

Praseodymium (Pr) is a rare earth element typically used as activators for providing strong red emissions under an excitation of ultraviolet light. Moreover, because of the close energy separation between the $^1S_0$ level and the lowest edge of

the 4f5d configuration, its emission is strongly dependent on the position of the 4f5d configuration, which is extremely influenced by the characteristics of the host [22,23]. Accordingly, the emissions of Pr^{3+} have been widely used as a structural transition probe for investigating phase transition of ferroelectric hosts that induces crystal-symmetry changes [24]. On the other hand, small amounts of rare earth ions have been shown to be beneficial to the good electrical properties of BNT-based ferroelectric ceramics [25,26]. In this work, we thus fabricate $0.93(Bi_{0.5}Na_{0.5})TiO_3$-$0.07BaTiO_3$ ceramics doped with 0.25 mol% Pr (abbreviated as Pr-BNTBT) with the aims of not only engendering strong PL emissions but also retaining the good piezoelectric properties. To reduce the volatilization losses of Bi and Na for improving the piezoelectric properties, Li_2CO_3 is used as a sintering aid for fabricating the ceramics at low sintering temperatures.

2. Experimental

$0.93(Bi_{0.5}Na_{0.5})TiO_3$-$0.07BaTiO_3$ ceramics doped with 0.25 mol% Pr^{3+} and x mol% Li_2CO_3 (abbreviated as Pr-BNTBT-Li-x, x = 0, 0.5, 1 and 2) were prepared by a conventional ceramic fabrication technique using analytical-grade carbonate or metal oxide powders: Na_2CO_3 (99.5%), Bi_2O_3 (99.9%), TiO_2 (99.9%), $BaCO_3$(99.5%), Pr_6O_{11} (99.9%) and Li_2CO_3 (99%). The powders in the stoichiometric ratio of Pr-BNTBT were mixed thoroughly in ethanol using zirconia balls for 8 h, and then dried and calcined at 850°C for 2 h. After the calcination, Li_2CO_3 powders were added. The mixture was then ball-milled again for 8 h, mixed thoroughly with a polyvinyl alcohol binder solution and then uniaxially pressed into disk samples with a diameter of 12 mm. The disk samples were finally sintered at 960-1200°C for 8 h in air. Silver electrodes were fired on the top and bottom surfaces of the sintered samples. The

samples were poled under a dc field of 5 kV/mm at 60˚C in a silicone oil bath for 30 min.

The crystallite structures of the samples were examined using X-ray diffraction (XRD) analysis with CuK_{α} radiation (SmartLab; Rigaku, Tokyo, Japan). The microstructures were observed using a field emission scanning electron microscope (FESEM) (JSM-6490; JEOL, Tokyo, Japan). The dielectric constants ε_r and dielectric loss tan δ were measured using an impedance analyzer (HP 4194A, Agilent Technologies Inc., Palo Alto, CA). A conventional Sawyer-Tower circuit was used to measure the polarization hysteresis (P-E) loop at 10 Hz. The piezoelectric coefficient d_{33} was measured using a piezo-d_{33} meter (ZJ-3A, Institute of Acoustics, Chinese Academy of Sciences, Beijing, China). The PL excitation and emission spectra were measured using a spectrophotometer (FLSP920, Edinburgh Instruments, UK), using a 450-W Xenon lamp as the excitation source. All the spectroscopic measurements were conducted at room temperature, and all the ceramic specimens were of the same thickness.

3. Results and discussions

The optimum sintering temperature for each Pr-BNTBT-Li-x ceramic has first been determined based on the observed dielectric and piezoelectric properties, giving the results summarized in Table 1. As compared to the Pr-BNTBT-Li-0 ceramic, the sintering temperature for the ceramics with $x > 0$ is lower and the range is narrower [27]. For each ceramic, if the sintering temperature is below its optimum value, it is not well densified and thus cannot be poled because of the high dielectric loss (typically > 10%). On the other hand, substantial degradation in dielectric and piezoelectric properties are resulted when the sintering temperature is higher than the

optimum value. As shown in Table 1, the (optimum) sintering temperature is lowered considerably from 1200°C to 960°C by the addition of 1 mol% Li_2CO_3 while only a slight decrease (~8%) in d_{33} is induced. Because of the slower mass transportation resulted from the low sintering temperature, a longer sintering (4 h) is required to complete the densification; otherwise, a porous structure and then a high tanδ will be obtained. The retained high d_{33} value is partly attributed to the reduced volatilization losses of Bi and Na resulted from the low sintering temperature, and partly attributed to the dense structure as exemplified by the SEM micrographs shown in Fig. 1. The observed densities for all the ceramics are high (5.78 - 5.82 g/cm^3), reaching about 96% of the theoretical densities [28]. The ceramics also possess high ε_r (~1600) and low tan δ (6%), both substantiating the dense structure obtained from the low temperature sintering. Apparently, the tan δ of a partially densified ceramic will increase significantly while its ε_r will decrease because of the high content of pores (i.e., air). As shown in Fig. 1, the grains of the low temperature-sintered ceramics become slightly smaller, which is partly attributed to the slow mass transportation resulted from the low sintering temperature.

The XRD patterns of the Pr-BNTBT-Li-x ceramics sintered at their optimum sintering temperatures are shown in Fig. 2, in which the XRD pattern of a BNTBT ceramic is also shown for comparison. All the ceramics possess a perovskite structure [6,11] and no impurity phases are observed within our detection limit, suggesting that both Li^+ and Pr^{3+} have diffused into the lattices. A splitting of the (202)/(200) diffraction peaks is observed for all the ceramics, confirming the co-existence of the rhombohedral and tetragonal phases. Because of the similar ionic radii of Pr^{3+} (1.34 Å, CN = 12) and the A-site ions (1.39 Å, average), no significant shift of the peaks is observed between the BNTBT and Pr-BNTBT-Li-0 ceramics. The ionic radii of Bi^{3+},

Na^+ and Ba^{2+} for CN = 12 are 1.36 Å, 1.39 Å and 1.6 Å, respectively [29]. On the other hand, the (202)/(200) diffraction peaks shift slightly to lower angles for the Pr-BNTBT-Li-x ceramics with x > 0. Because of the similar ionic radii, Li^+ (1.41 Å, CN = 12) should enter the A-sites of the ceramics. However, it has been shown that Li^+ will enter the B-sites of BNT-based ceramics in spite of the larger ionic difference (0.76 Å vs 0.61 Å, CN = 6) if its concentration is higher than 0.75 mol% [30]. Accordingly, it is suggested that Li^+ has entered the A-site of the ceramics with $x \leq 0.5$ and entered the B-site of the ceramics with x > 0.5. In both cases, the substitution (with larger ions) will lead to an expansion in lattices and then a shift of the diffraction peaks towards lower angles as shown in Figure 2. Oxygen vacancies will be formed because of the different valence states for maintaining the charge neutrality, which on the other hand will induce shrinkage of the lattices [30]. However, as illustrated by the observed shifting, it should be completely compensated. Oxygen vacancies can also increase the ionic lattice-diffusion coefficient and promote densification [20,31], and thus realizing the well sintering at low temperatures.

Fig. 3 shows the temperature-dependent ε_r and tan δ for the poled Pr-BNTBT-Li-0 and Pr-BNTBT-Li-1 ceramic. Similar to other BNT-based ceramics, the Pr-BNTBT-Li-0 ceramic exhibits two distinctive anomalies in the $\varepsilon_r(T)$ curve, i.e., a frequency-dispersive shoulder at ~150°C and a broad maximum peak at 270°C, both demonstrating the relaxor characteristics of the ceramic (Fig. 3a) [32,33]. On the other hand, a very weak peak corresponding to the transition between non-ergodic and ergodic relaxor state is barely observed at ~40°C (T_d, depolarization temperature) in the tan $\delta(T)$ curve, which agrees with similar works reported elsewhere [34]. This then indicates that, as also substantiated by the high d_{33} (165 pC/N), the ceramic is in the non-ergodic state at room temperature [32,33]. Unlike typical ferroelectric

materials, ferroelectric relaxors contain polar nano-regions (PNRs) that can similarly be aligned under a sufficient high electric field. Upon the removal of the electric field, the aligned PNRs of the non-ergodic relaxors are retained and thus exhibiting piezoelectric effect. On the other hand, the aligned PNRs of the ergodic relaxors will relax back to the randomly oriented state. In other words, ergodic relaxors cannot be effectively poled to engender piezoelectric properties. As indicated by the low T_d and weakness of the peak (Fig. 3a), the degree of ergodicity of the Pr-BNTBT-Li-0 ceramic is not very low, i.e., it still contains a small portion of ergodic relaxor. This consequently gives rise to a slightly constricted P-E loop as shown in Fig. 4. As the composition ratio of the rhombohedral and tetragonal phases is decreased by the Li-substitution [35], the Pr-BNTBT-Li-1 ceramic exhibits a single dielectric anomaly (Fig. 3b). Moreover, the tan δ-peak at T_d becomes stronger and shifted to a higher temperature (~70°C), suggesting that the degree of ergodicitiy is reduced. Accordingly, the constriction of the P-E loop diminishes (Fig. 4) and a larger remanent polarization is obtained (22.1 vs 12.6 $\mu C/cm^2$), which in turn contributes to the high d_{33} value of the ceramic (Table 1). The decrease in ergodicity is attributed to the lattice expansion and distortion induced by the Li-substitution, which strengthen the internal field among the polar nano-regions of the relaxor ceramics.

The photoluminescence excitation spectrum (PLE) of the Pr-BNTBT-Li-1 ceramic has first been measured, as an example, for determining the optimum wavelength of the excitation source. As illustrated in Fig. 5a, via monitoring the typical emission (610 nm) of Pr^{3+}, three groups of excitation peaks attributed to the inter-4f transitions from the $^3H_4$ ground level to the $^3P_2$, $^3P_1$ and $^3P_0$ levels are observed at 448, 468 and 480 nm, respectively (Fig. 6). Based on the results that the highest PLE intensity observed at 468 nm, an excitation source with the same

wavelength has been used for measuring the PL spectra. As shown in Fig. 5b, all the ceramics exhibit a strong wide emission band in the range of 590 to 540 nm and a weak emission peak at ~655 nm, which are attributed to the 4f-4f transitions $^1D_2 \rightarrow {}^3H_4$ and $^3P_0 \rightarrow {}^3F_2$, respectively. As x increases, the PL intensity increases and reaches a maximum at x = 1. This is attributed to the reduction in structural symmetry arisen from the lattice expansion and distortion induced by the Li-substitution. It has been shown that the crystal field of a host with lower symmetry contains normally more uneven components around the dopant ions, which can enhance the electronic coupling between 4f energy levels and higher 4f5d configuration and thus increase the f-f transition probabilities of the ions [22,23]. On the other hand, the decrease in PL intensity for the ceramic with x > 1 should be attributed to its larger amount of oxygen vacancies, which has been shown to be effective in quenching visible luminesces via acting as electron traps [36].

The decay curves of emission at 610 nm for the Pr-BNTBT-Li-x ceramics under the excitation of 468 nm are shown in Figure 7. Good agreement are generally obtained in fitting the data to a single exponential function $I = I_o\exp(-t/\tau)$, where τ is the emission lifetime and I_o is the initial emission intensity. As also shown in Figure 7, the calculated τ increases with increasing x and then decreases after reaching a maximum at x = 1. The prolonged lifetime should largely be attributed to the decrease in non-radiative transition induced by the lattice distortion [37]. On the other hand, the adverse effect of oxygen vacancies for shortening the lifetime via non-radiative energy transfer becomes dominated for the ceramic with x > 1 [38].

4. Conclusions

Low-temperature sintering of Pr-doped BNTBT multifunctional ceramics has been realized using Li_2CO_3 as a sintering aid. The ceramics possess good dielectric, ferroelectric, piezoelectric and PL properties as well as a dense structure. Arisen from the substitution of Li^+, oxygen vacancies as well as lattice expansion and distortion are produced. The low-temperature sintering is realized owing to the oxygen vacancies that increase the lattice-diffusion coefficient and then promote densification. On the other hand, the lattice expansion and distortion break the ergodicity via strengthening the internal field among the nano-polar regions of the relaxor ceramics. A large remanent polarization is thus produced and the good piezoelectric properties of the low-temperature-sintered ceramics are retained. The lattice expansion and distortion also reduce the structural symmetry and then increase the uneven components of the crystal fields around Pr^{3+}. As a result, the PL emissions of the ceramics are enhanced. Based on the good properties, the ceramics are expected to become promising materials for use various optoelectronic applications, with the additional advantages of energy saving and environmental protection.

Acknowledgements

This work was supported by the Research Grants Council of the Hong Kong Special Administrative Region (Project No. PolyU 5170/13E).

References

[1] D.F. Peng, X.S. Wang, C.N. Xu, X. Yao, J. Lin, T.T. Sun, J. Am. Ceram. Soc. 96 (2013) 184-190.

[2] L.T. Canham, Appl. Phys. Lett. 57 (1990) 1046-1048.

[3] H. Lu, C.W. Bark, D.E. Ojos, J. Alcala, C.B. Eom, G. Catalan, A. Gruverman, Science 336 (2012) 59-61.

[4] Q.Y. Yue, L.H. Luo, X.J. Jiang, W.P. Li, J. Zhou, J. Alloy. Compd. 610 (2014) 276-280.

[5] J.T. Zeng, Z.H. Wei, Y.L. Huang, T. Tsuboi, L.Y. Zheng, W. Ruan, S.W. Wang, G.R. Li, J. Am. Ceram. Soc. 95 (2012) 2573–2578.

[6] T. Takennaka, K. Maruyama, K. Sakata, Jpn. J. Appl. Phys., Part 1 30 (1991) 2236-2239.

[7] H. Muramatsu, H. Nagata, T. Takenaka, Jpn. J. Appl. Phys. 55 (2016) 10TB07.

[8] Y.M. Li, W. Chen, J. Zhou, Q. Xu, H.J. Sun, R.X. Xu, Mater. Sci. Eng. B 112 (2004) 5-9.

[9] X.X. Wang, K.W. Kwok, X.G. Tang, H.L.W. Chan, C.L. Choy, Solid State Commun. 129 (2004) 319-323.

[10] D. Lin, D. Xiao, J. Zhu, P. Yu, Appl. Phys. Lett. 88 (2006) 062901.

[11] C. Xu, D. Lin, K.W. Kwok, Solid State Sci.10 (2008) 934-940.

[12] T. Takenaka, H. Nagata, Y. Hiruma, IEEE Trans. Ultrason. Ferroelectr. Freq. Control 56 (2009) 1595-1612

[13] Z.Z. Huang, H.L.W. Chan, K.W. Kwok, C.L. Choy, J. Mater. Sci. 35 (2000) 1793-1797.

[14] K. Wang, J.F. Li, J. Adv. Ceram. 1 (2012) 24–37.

[15] D.E. Wittmer, R.C. Buchanan, J. Am. Ceram. Soc. 64 (1981) 485-490.

[16] X. Wang, K. Murakami, S. Kaneko, Jpn. J. Appl. Phys. 39 (2000) 5556-5559.

[17] R. Mazumder, A. Sen, J. Eur. Ceram. Soc. 28 (2008) 2731-2737.

[18] G.F. Fan, M.B. Shi, W.Z. Lu, Y.Q. Wang, F. Liang, J. Eur. Ceram. Soc. 34 (2014) 23-28.

[19] Y.D. Hou, L.M. Chang, M.K. Zhu, X.M. Song, H. Yan, J. Appl. Phys. 102 (2016) 084507.

[20] R.M. German, P. Suri, S.J. Park, J. Mater. Sci. 44 (2009) 1-39.

[21] D.L. Corker, R.W. Whatmore, E. Ringgaard, W.W. Wolny, J. Eur. Ceram. Soc. 20 (2000) 2039-2045.

[22] F. You, S. Huang, C. Meng, D. Wang, J. Xu, Y. Huang, G. Zhang, J. Lumin. 122-123 (2007) 58-61.

[23] W.W. Piper, J.A. DeLuca, F.S. Ham, J. Lumin. 8(4) (1974) 344-348.

[24] P. Zhang, M. Shen, L. Fang, F. Zheng, X. Wu, J. Shen, H. Chen, Appl. Phys. Lett. 92 (2008) 222908.

[25] X.X. Wang, H.L.W. Chan, C.L. Choy, Solid State Commun. 125 (2003) 395-399.

[26] M. Zannen, A. Lahmar, B. Asbani, H. Khemakhem, M. El Marssi, Z. Kutnjak, M. Es Souni, Appl. Phys. Lett. 107 (2015) 032905.

[27]

[28] M. Chandrasekhar, P. Kumar, Ceram. Int. 41 (2015) 5574-5580.

[29] R.D. Shannon, Acta Cryst. A32 (1976) 751-767.

[30] N. Lei, M. Zhu, P. Yang, L. Wang, L. Wang, Y. Hou, H. Yan, J. Appl. Phys. 109 (2011) 054102.

[31] M. Valant, D. Suvorov, R.C. Pullar, K. Sarma, N.M. Alford, J. Eur. Ceram. Soc. 26 (2006) 2777-2783.

[32] W. Jo, S. Schaab, E. Sapper, L.A. Schmitt, H.J. Kleebe, A.J. Bell, J. Rödel, J. Appl. Phys. 110 (2011) 074106.

[33] W. Jo, R. Dittmer, M. Acosta, J. Zang, C. Groh, E. Sapper, K. Wang, J. Rödel, J. Electroceram. 29 (2012) 71–93.

[34] Q. Yao, F. Wang, F. Xu, C.M. Leung, T. Wang, Y. Tang, X. Ye, Y. Xie, D. Sun, W. Shi, ACS Appl. Mater. Interfaces 7 (2015) 5066-5075.

[35] G. Viola, R. McKinnon, V. Koval, A. Adomkevicius, S. Dunn, H. Yan, J. Phys. Chem. C 118 (2014) 8564−8570.

[36] C.M. Lau, X. Wu, K.W. Kwok, J. Appl. Phys. 118 (2015) 034107.

[37] Q. Sun, X. Chen, Z. Liu, F. Wang, Z. Jiang, C. Wang, J. Alloys Compd. 509 (2011) 5336–5340.

[38] Y. Zhang, J. Hao, C. L. Mak, and X. Wei, Opt. Express 19 (2011) 1824–1829.

Table 1 Sintering conditions and physical properties for the Pr-BNTBT-Li-x ceramics. The experimental error for the physical properties is ±5%.

x	Sintering Temperature (°C)	Sintering Time (h)	ε_r	tan δ (%)	d_{33} (pC/N)	Grain size (nm)
0	1200	2	1490	5.2	180	450
0.5	1060	4	1540	4.8	170	300
1	960	4	1650	5.6	170	430
2	960	4	1560	5.1	110	410

Figure Captions

Fig. 1 SEM micrographs of the Pr-BNTBT-Li-x ceramics sintered at their optimum sintering conditions.

Fig. 2 XRD patterns of the Pr-BNTBT-Li-x ceramics.

Fig. 3 Temperature-dependent ε_r and tan δ for the poled Pr-BNTBT-Li-x ceramics.

Fig. 4 P-E hysteresis loops of the Pr-BNTBT-Li-x ceramics with x = 0 and 1.

Fig. 5 (a) Photoluminescence excitation spectrum of the Pr-BNTBT-Li-1 ceramic. (b) Photoluminescence spectra of the Pr-BNTBT-Li-x ceramics.

Fig. 6 Energy level diagram of Pr^{3+} ion.

Fig. 7 Decay curves of emission at 610 nm for the Pr-BNTBT-Li-x ceramics.

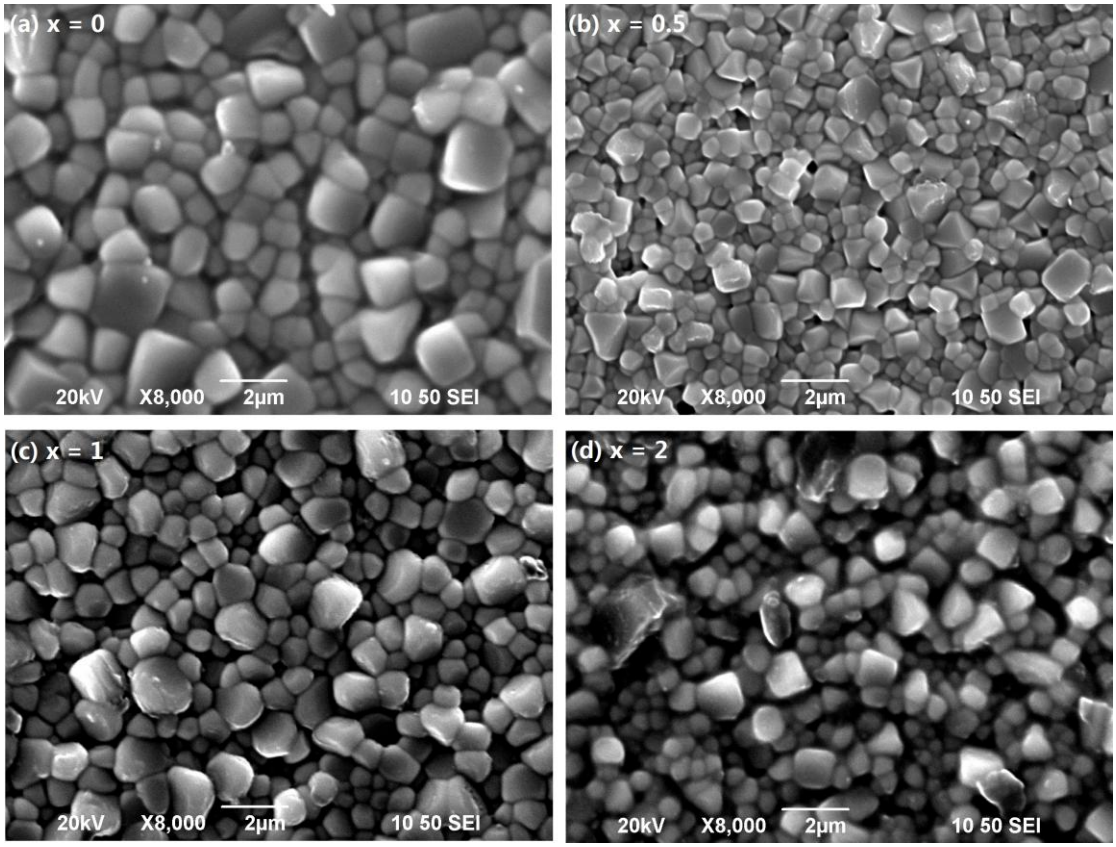

Fig. 1 SEM micrographs of the Pr-BNTBT-Li-x ceramics sintered at their optimum sintering conditions.

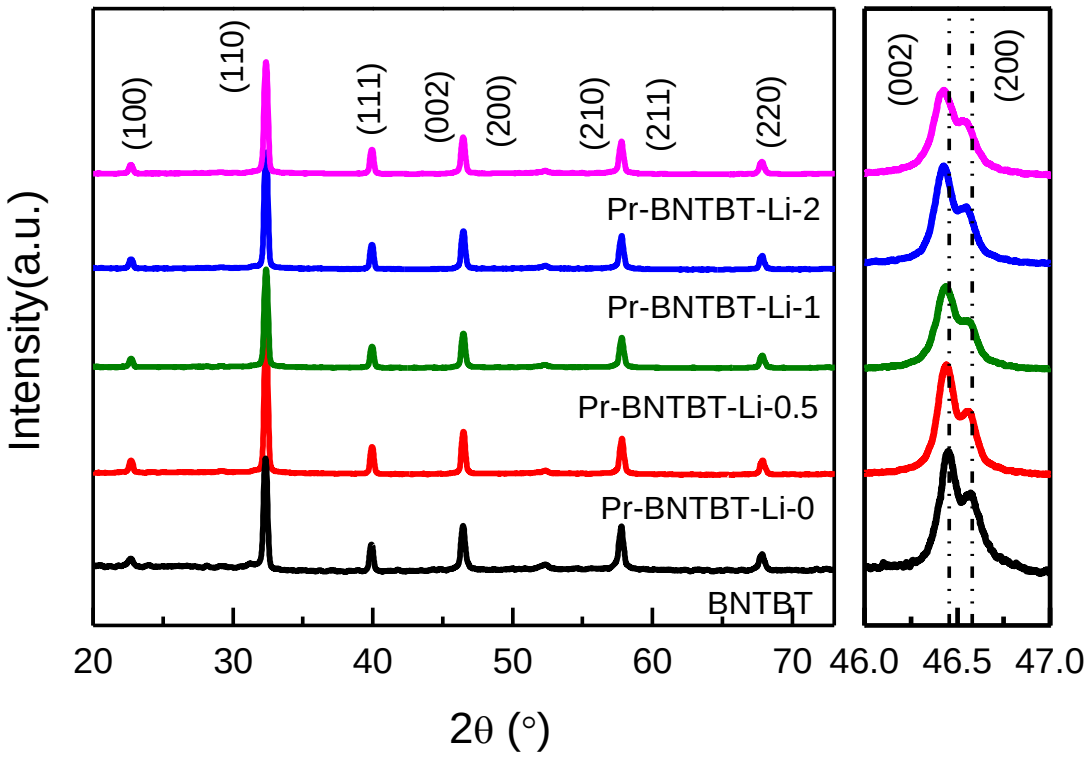

Fig. 2 XRD patterns of the Pr-BNTBT-Li-x ceramics.

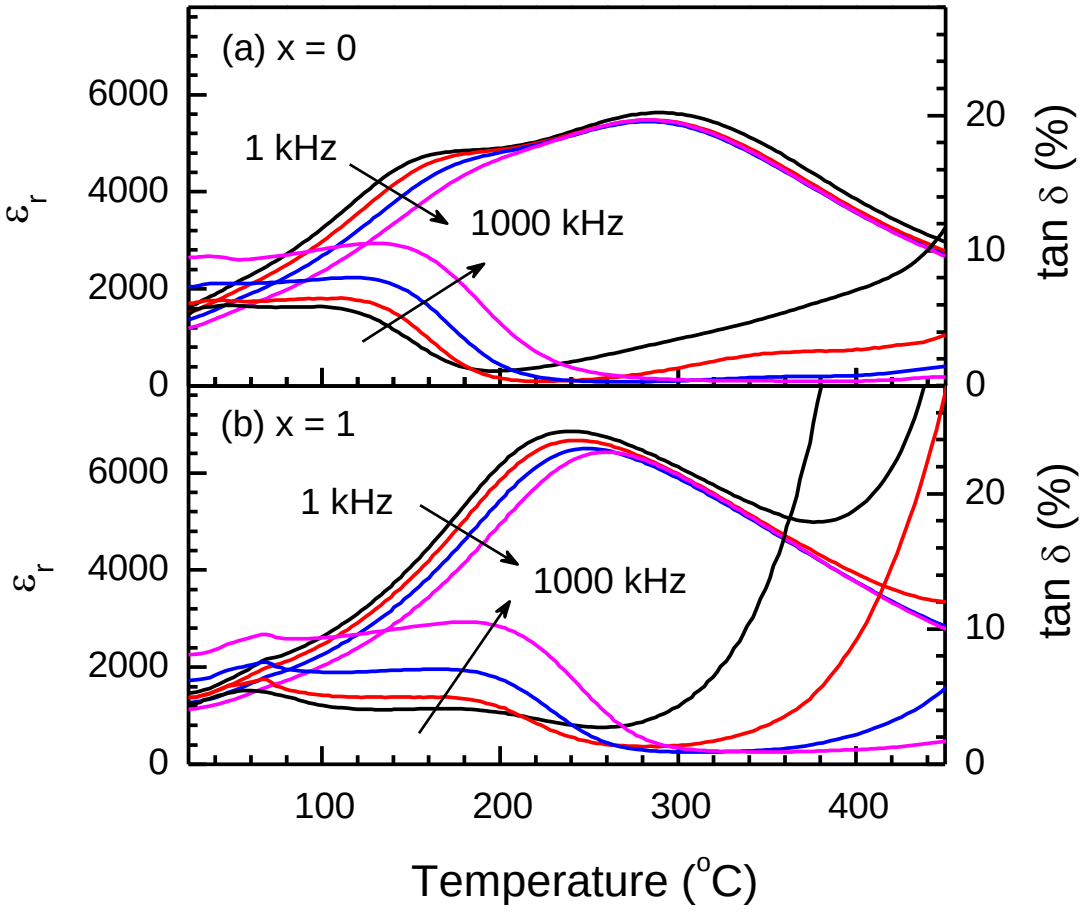

Fig. 3 Temperature-dependent εr and tan δ for the poled Pr-BNTBT-Li-x ceramics.

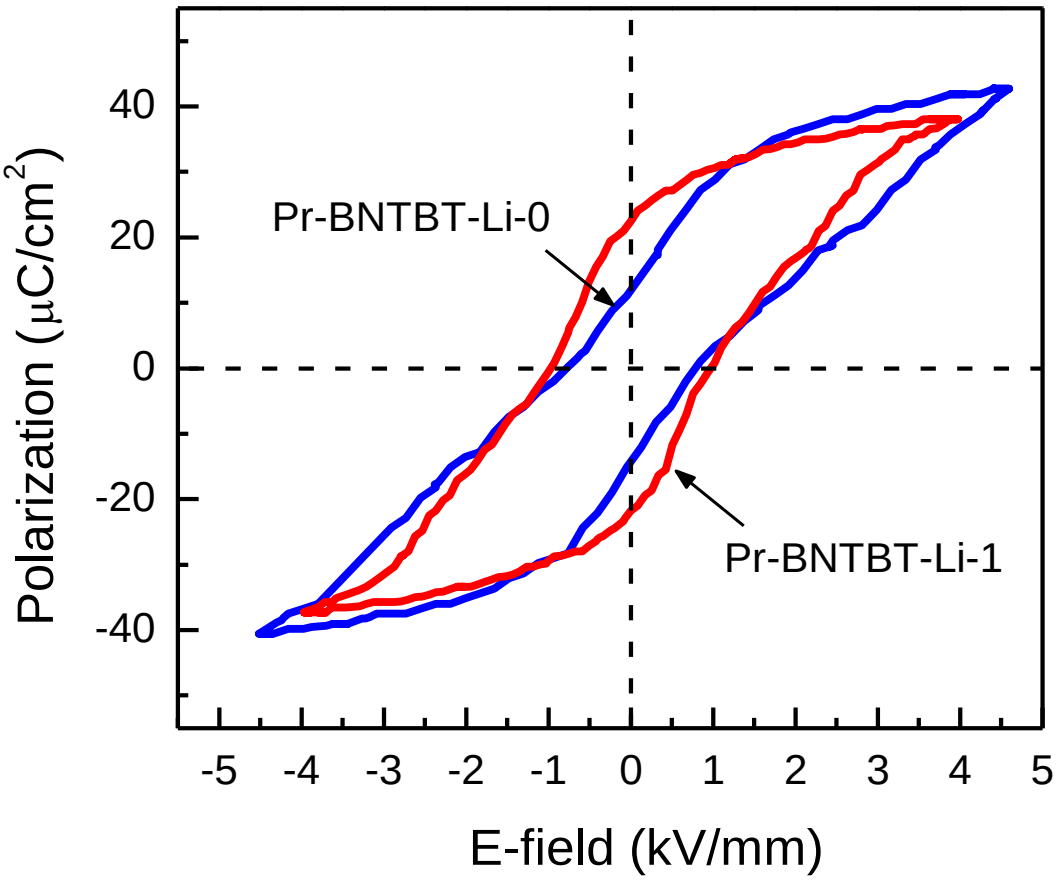

Fig. 4 P-E hysteresis loops of the Pr-BNTBT-Li-x ceramics with x = 0 and 1.

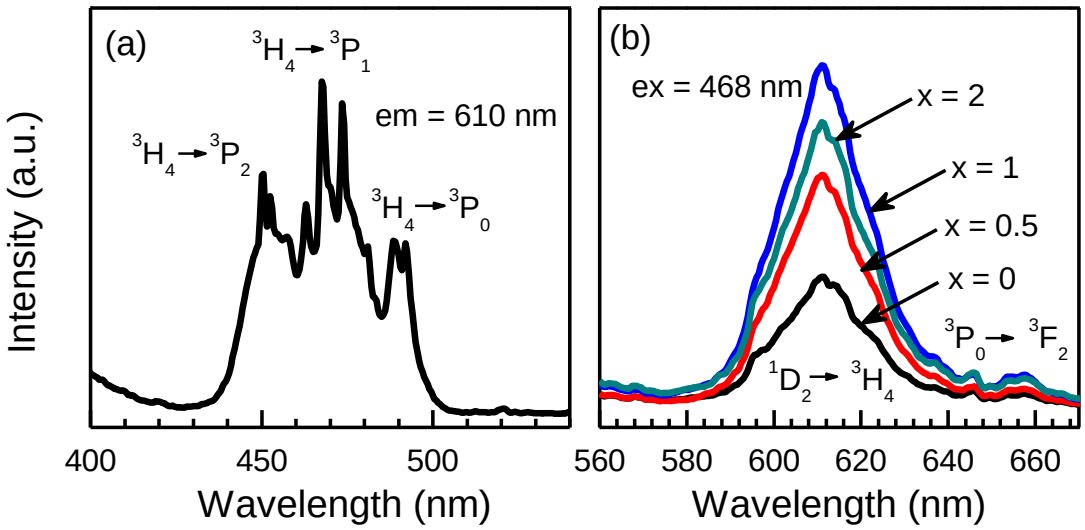

Fig. 5 (a) Photoluminescence excitation spectrum of the Pr-BNTBT-Li-1 ceramic.

(b) Photoluminescence spectra of the Pr-BNTBT-Li-x ceramics.

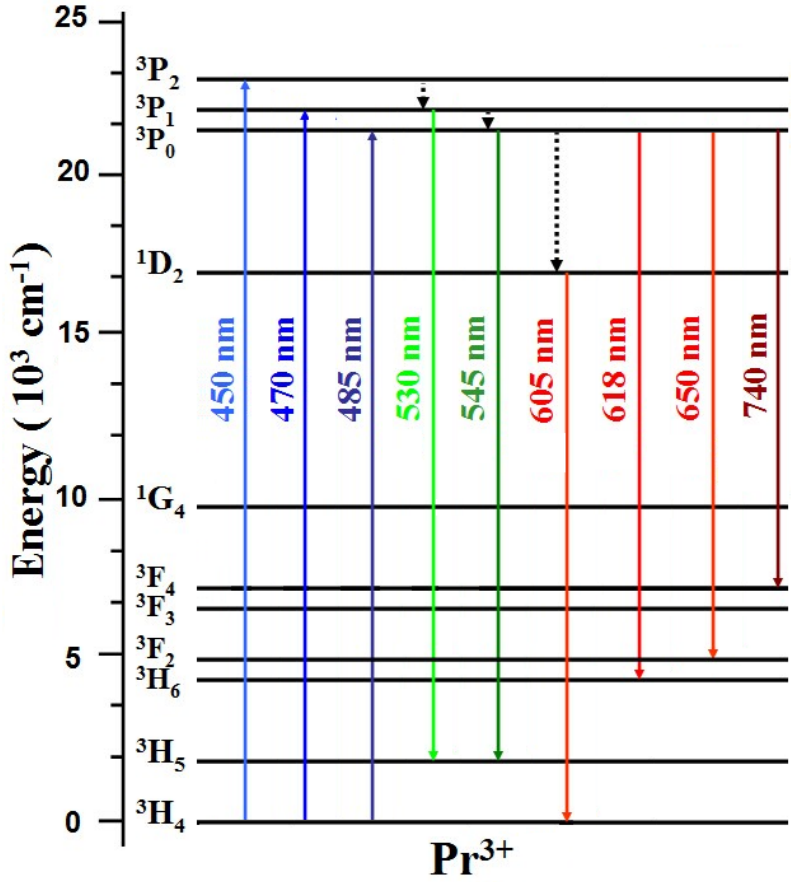

Fig. 6 Energy level diagram of Pr^{3+} ion.

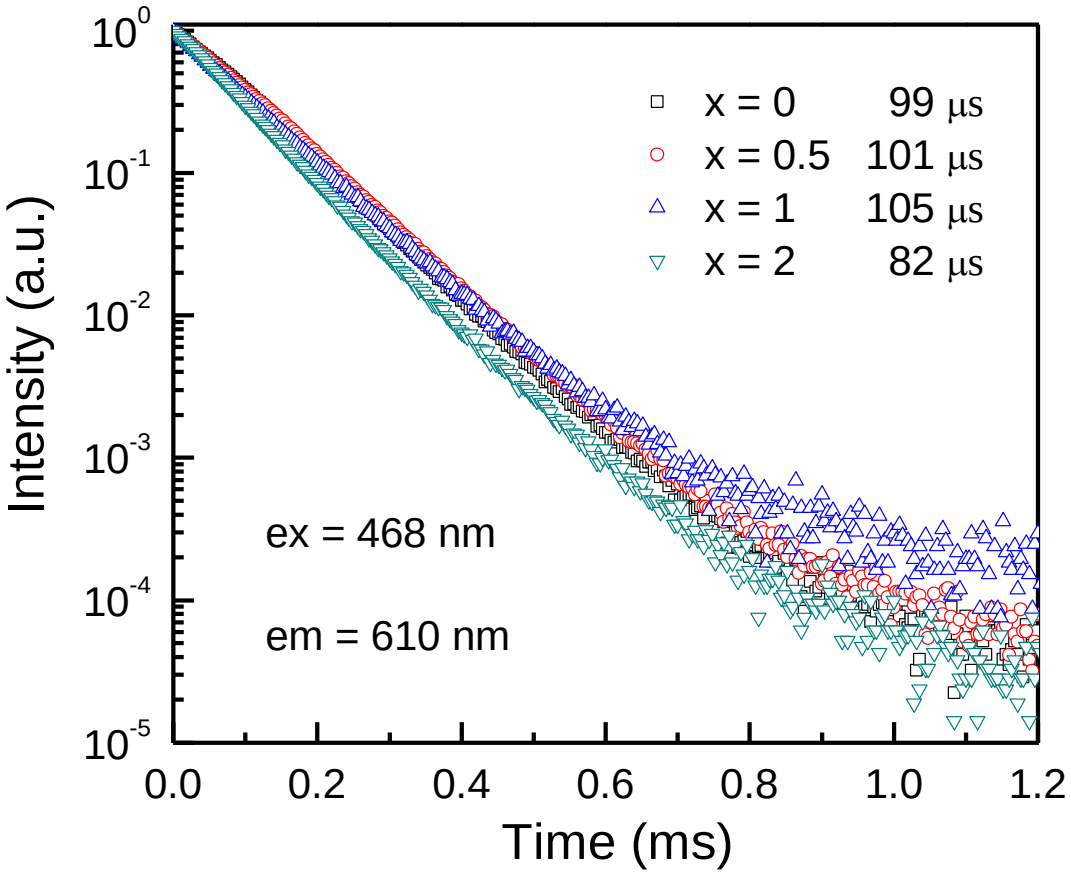

Fig. 7 Decay curves of emission at 610 nm for the Pr-BNTBT-Li-x ceramics.